Stark broadening of Balmer lines in the density range (2–8) $\times 10^{14}$ cm^{-3}*

Roger D. Bengtson and Gerald R. Chester†
Department of Physics, The University of Texas at Austin, Austin, Texas 78712
(Received 24 November 1975)

Experimental profiles of the hydrogen Balmer lines (H_γ-H_{10}) have been measured over the density range (2–8) $\times 10^{14}$ cm^{-3} and compared with theoretical profiles. Electron densities were measured using a multipass interferometer, while plasma homogeneity was demonstrated using a Langmuir probe. Electron temperatures were in the range 1–2.0 eV. The electron density as deduced from line profiles tended to be as much as 10% lower than that from the interferometer at higher densities. At lower densities, the two methods agreed to within experimental error. Evidence for asymmetries on the line wings was noted.

I. INTRODUCTION

Accurate experimental studies to date of hydrogen Stark broadening have generally been confined to either low-[1] ($n_e \approx 10^{13}$ cm^{-3}) or high-[2,3] density ($n_e > 10^{16}$ cm^{-3}) plasmas. A recent investigation[4] compared experimental profiles of H_β from an arc of density 4×10^{14}–3×10^{15} cm^{-3} with theoretical profiles. The main reasons for the lack of experimental data in the intermediate-density region ($n_e \sim 10^{14}$–10^{15} cm^3) are the difficulties in producing a homogeneous plasma of known characteristics with sufficient intensity and time duration so that accurate measurements of the profiles can be obtained. These problems have been solved by using a large-Z discharge, which was originally designed for shock-wave studies.[5] In the present work, the preheat phase of this apparatus has been used to generate a homogeneous reproducible afterglow which spans the density region $10^{14} < n_e < 10^{15}$ cm^{-3}. Unlike other devices which produce afterglow times of typically 10 μsec, we obtained afterglow times of 300 μsec with sufficient radiation intensity to make reliable diagnostic and profile measurements.

The intermediate-density region is highly relevant in checking the basic assumptions of hydrogen-line-broadening theory, since in this regime the effects of multiparticle correlations are minimized. Estimated theoretical errors in the Stark profiles of the first four Balmer lines from approximations in the theory are less than 8%.[6,7]

Furthermore, some experimental problems are minimized using an intermediate-density plasma rather than a high-density plasma. The continuum scales as the square of electron density, which may superimpose a significant continuum background contribution on the line wings, and thereby create difficulty in delineating accurately the far wings of the profiles. High-density studies are also limited by line merging, which restricts the study to the first three or four Balmer lines. In the low-density region, the Stark effect can be seriously rivaled by Van der Walls and/or Doppler broadening. In the density region in which we are working, Stark broadening dominates all Balmer profiles past H_α, line merging does not affect profiles until past H_{10}, and the density is low enough that the continuum contributions in the line wings are small.

It is the purpose of this work to provide a detailed systematic study of the Balmer spectrum $H_\gamma - H_{10}$ in the intermediate-density region, and to compare the experimental profiles with the recent theoretical treatments of Smith, Cooper, and Vidal[6] (VCS), and Kepple and Griem[7] (KG).

II. EXPERIMENT

A. Apparatus

The experiment was performed on The University of Texas oblique shock machine,[5] normally used to study shock waves in plasmas. In the present work, the apparatus was used as a Z discharge.

Figure 1 shows a schematic of the experiment. Plasma generation was accomplished by discharging a 360-μF capacitor bank through 20 mTorr of 99.999%-pure molecular-hydrogen gas. This preheat capacitor was initially charged to 6.3 kV; two stainless-steel endplates served as the electrodes for the damped oscillating current. A Pyrex tube 93 cm long and 45 cm in diameter confined the gas between the electrodes. The ringing time of the preheat circuit was 160 μsec per cycle. Current flowed for three half-cycles before it was clamped. During this phase, the gas was heated and ionized, forming a plasma with an electron density ~10^{15} cm^{-3} and a temperature ~2 eV. The observation period began with the clamping of the preheat current and lasted for 300 μsec. The plasma was immersed in a spatially uniform and temporally constant 500 G magnetic field parallel to the tube axis.

Data were taken by viewing the plasma axially along two optical paths, both of which were located

10 cm from the plasma center. Each of the endplates or electrodes contained two Pyrex windows. One set of windows was placed at the Brewster angle for 3.39-μm radiation to be used for an eight-pass laser interferometer, which monitored the electron density during the observation period. The other set, located at the same radius but rotated by 90° relative to the first set, was used for spectroscopic observations. This arrangement required the assumption of azimuthal symmetry for the plasma analysis.

Radiation emitted from the plasma was focused onto the entrance slit of a $\frac{1}{2}$-m Ebert spectrometer. The instrument was located approximately 400 cm from the exit port to minimize the perturbation from the confining magnetic field on the photomultiplier. The radiation emitted by the plasma was attenuated by the Pyrex windows on the exit ports. Attenuation increased with the number of shots and with decreasing wavelength. We assumed that initially both the front and back windows were clean and transmission degenerated as deposits built up on the windows during the course of the experiment. The transmission coefficients were measured and incorporated into the analysis of the Stark profiles.[8] This correction, though small for each individual profile, was necessary for absolute intensity measurements and the construction of a complete Balmer spectrum. No window correction was needed for the laser interferometer data.

B. Diagnostics

The diagnostics of the plasma consisted not only of the usual measurement of electron temperature and density, but also axial homogeneity and emissivity. By establishing that the source is homogeneous and free of serious boundary-layer problems, the density and temperature measurements can be identified as true bulk properties of the plasma relevant to the region where the Stark profiles are formed.

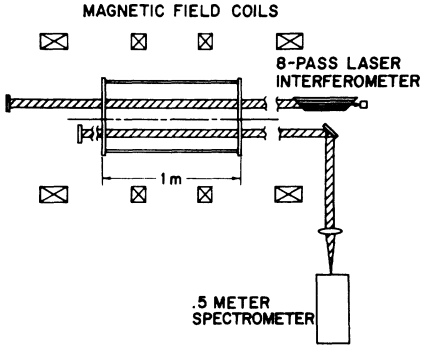

FIG. 1. Schematic of experiment.

1. Axial homogeneity

By using a large plasma source, one hopes that the effects of boundary layers on the emitted spectra can be reduced to the point of insignificance. Since the source is large enough to determine quantitatively the variation in plasma parameters along the optical path, a point-by-point measurement using a double Langmuir probe was performed. The probe consisted of two spherical platinum tips approximately 1 mm in diameter, with a spatial separation of approximately 5 mm. It was powered by a free-running sine-wave generator at 70 kHz, and a power amplifier to bias the probe tips. The use of an ac driving voltage on the probe aided in cleaning the probe surface and in reducing problems caused by secondary emission and arcing. The current between the probe tips was measured using a current transformer, while the voltage was measured by a similar current transformer measuring the current through a resistor in parallel with the probe tips. We followed the saturation current as a function of time and simultaneously displayed a complete probe curve on a second oscilloscope at one point in time. Since the afterglow lifetime was 300 μsec, each probe curve was taken while the plasma parameters were nearly constant in time. We could see no effect on the macroscopic variables of the plasma (current, density) by inserting the probe. It was found to be necessary to offset the probe tips from the probe body in order to produce a symmetric probe curve.

The relative electron density as a function of distance from the endplates at 150 μsec after current was clamped is shown in Fig. 2. Each datum point is the average of several shots with approximately the indicated error. The graph contains data taken from two separate data runs, using different probes and different current sources. From the envelope of the saturation current, we could also follow homogeneity as a function of time.

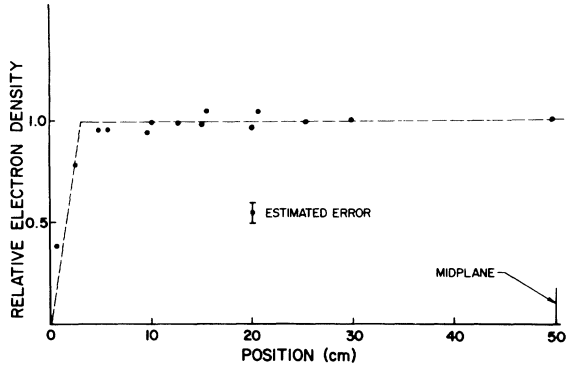

FIG. 2. Electron density as a function of axial distance in the afterglow of the Z discharge.

There was no apparent change in the spatial density distribution with time. The narrow boundary layers with a flat distribution within the body of the plasma indicate that the diffusion coefficient is not constant throughout the plasma. Density gradients were found only near the end walls. Plasma temperature dropped to about one-half its value at the center of the discharge tube approximately 2 cm from the wall. The scale length for the temperature drop was roughly the same as for the density change. Temperatures derived from the Langmuir-probe data were the same as those measured by spectroscopic methods, although with larger scatter and systematic error. We also measured the electron density back into the cavity formed by the Brewster-angle window. The plasma density dropped below probe sensitivity about 1 cm back into the cavity suggesting a very collisional boundary layer in which the diffusion parallel to the field and the diffusion perpendicular to the field are about the same. Paul *et al.*[9] using a similar discharge measured a boundary layer of only 1 cm in front of each electrode. While the boundary layer measured on our apparatus was about 2–3 cm, the bulk of the plasma (94%) had a density which was constant to within ±4%.

2. *Axial emissivity*

We also performed a measurement of the axial emissivity using a directional optical probe inserted into the plasma to verify that the boundary layers were not dominating or seriously altering the observed spectra. The results of this measurement indicated that the emission spectra were from the main body of the plasma and not from a narrow boundary layer. Axial emissivity was observed to increase slightly ($\lesssim$15%) at the endplate, which is consistent with the fact that the neutral particle density will increase at the wall to maintain pressure balance. The increase was localized to less than 5 cm, and for an optically thin plasma was not substantial enough to alter the observed spectra more than 2%. Thus we have a source that is both homogeneous in plasma parameters and uniform in emissivity for more than 94% of the optical path.

3. *Electron temperature*

Two techniques were used to measure the electron temperature of the plasma, namely, the line-to-continuum ratio and the continuum-to-continuum[10] ratio. Figure 3 shows the results of these measurements. No significant variation was noted during the period of data collection. The results were reproducible to within ±10%.

Line-to-continuum ratios for all the lines examined in this experiment (i.e., H_β–H_{10}) were taken and used to provide a temporal history of the electron temperature during the afterglow. The various lines yielded results which agreed typically to within ±10%, and no systematic variation was found which indicated any dependence on the diagnostic line employed. Despite this excellent agreement, it should be noted that the line-to-continuum technique does assume a local thermal equilibrium (LTE) plasma; namely, it assumes that the electrons have a Maxwellian distribution and the atomic-number densities are given by the Saha-Boltzmann distribution. The former assumption was not experimentally verified, but seems quite reasonable in light of the absence of large external electric fields and a Spitzer electron equilibration time ~0.5 nsec. The latter assumption was tested by measuring the atomic-state number densities and comparing them with the Saha-Boltzmann predictions calculated using electron temperatures measured from the line-to-continuum technique. It was found that the atomic states were overpopulated up to a factor of 6.

Although the relative-continuum technique does assume a Maxwellian electron distribution, it does not depend strongly on a Saha-Boltzmann distribution of atomic states. It then provides a viable test for the error introduced in the line-to-continuum technique by the Saha-Boltzmann assumption.

The intensity ratio for wavelengths 4500 and 3500 Å was measured and found to be consistently reproducible. Using the continuum tables published by Eberhagen and Lünow,[11] a temporal history of the electron temperature was found. Referring again to Fig. 3, one notes that the line-to-continuum measurement is typically 20% below the relative-continuum measurement, but in all cases it is

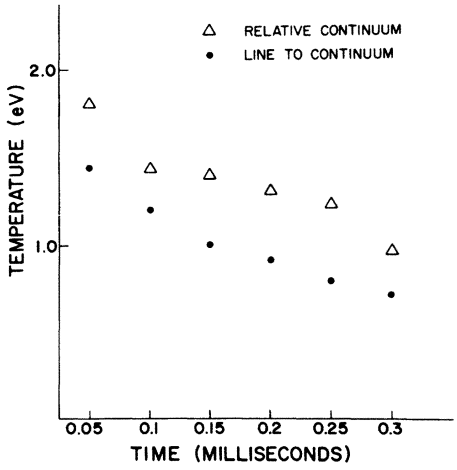

FIG. 3. Electron temperature as measured using the relative-continuum and line-to-continuum techniques.

within 40%. The data indicate that the atomic-state excitation temperature is somewhat lower than the electron temperature of the continuum electrons. The variance in the two temperature measurements is not serious since the Stark profiles are very weakly dependent on electron temperature. In our analysis we assumed that the temperature of the electrons is given by the relative-continuum method.

A third estimate of the plasma temperature was made by converting the intensity at the peak of the optically thick H_α to an equivalent blackbody temperature. This "blackbody" temperature is always lower than the line-to-continuum and relative-continuum techniques as demanded by thermodynamic considerations. However, the observation that the blackbody temperature is nearly the same as other temperatures is a strong argument that we are observing the bulk of the plasma and not just a cool dense boundary layer.

4. Electron density

The critical parameter in the analysis of Stark profiles is the electron density. Measurement of electron density was made using two independent techniques: laser interferometry and absolute continuum intensity.

The laser-interferometer technique is based on monitoring the change in the plasma index of refraction as a function of time. For a plasma the index of refraction may be written as

$$n = 1 - \tfrac{1}{2}(\omega_p/\omega)^2 + 2\pi \sum_i a_i(\omega) N_i, \qquad (1)$$

where $\omega_p = 5.6 \times 10^4 \sqrt{N_e}$ is the electron plasma frequency; ω is the frequency of the laser beam; $a_i(\omega)$ is the polarizability of the ith state at the laser frequency; and N_i is the number density in the ith state.

The second term in Eq. (1) represents the contributions from electrons and the third term represents contributions from other species. Neutral contributions can be significant when either the polarizability is large or the population of atomic states is large. Calculations of the extreme cases which apply to the present experiment predict that neutral hydrogen contributions are always less than 1% of the electron contributions.[8] Other contributions can come from impurity atoms and/or molecules which possess transitions close to the laser frequency, and hence, cause the polarizability to be large. Ideally, one would like to observe the spectrum in the 3.39-μm region to determine if such phenomenon occurred. We assumed that the index of refraction reflects only electron density changes and can be used to measure the temporal history of this quantity in the afterglow plasma.[8] Support for this assumption is obtained by the credible agreement between the results of this method and those of the absolute-intensity technique.

The laser was set up to allow eight passes of the beam through the plasma before reflection back into the laser cavity. Fringe shifts were monitored by an infrared detector mounted behind the laser cavity. Each fringe shift corresponded to a change in density of 8.3×10^{13} cm^{-3}. It should be noted that the plasma length and profile used in these calculations were those determined from the axial-density-probe measurement.

Fringe-shift data were reduced by minimizing the deviation to an exponential decay of density with time, while adding or subtracting fractions of a fringe to account for the uncertainty in the final phase of the interferometer. We found that on the average about a half fringe was added to our estimated fringe pattern for each data set. This was probably caused by inadequate low-frequency response of the detector.

Results of the electron density measurement using the laser interferometer are shown in Fig. 4. The solid line represents the average density decay

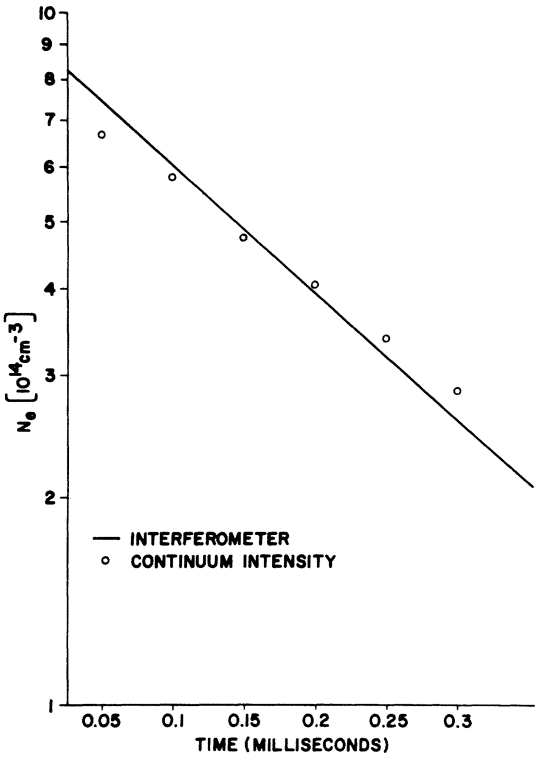

FIG. 4. Electron density as measured by interferometer, and by absolute intensity of the Balmer continuum.

measured with the interferometer over the period in which data were taken. Fringe-shift data were taken simultaneously with line-profile data. This served two purposes: First, since data were taken on a shot-to-shot basis, anomalous electron density behavior during a day's operation could be noted, and second, any systematic changes from day to day in the system could be monitored by comparing the average electron density from other days of operation. Both shot-to-shot and day-to-day variations were found to be insignificant; typical shot-to-shot scatter was less than 5%. Observable distortions due to mirror vibrations were on a slower time scale than the plasma decay time. Historically, interferometer density measurements have been assigned an error of half of a fringe shift due to the uncertainty in the final phase between the standing wave in the laser cavity and the beam reflected back into the cavity. This implies an average accuracy of approximately 5%, which is of the same order as the error estimated from the reproducibility.

Another independent measurement of the electron density was from the absolute intensity[11] of the continuum measured at five different wavelengths. Expressed as a function of electron density (N_e), temperature (T_e), and wavelength (λ), the continuum emissivity is given by

$$\epsilon = \frac{32\pi^2}{3\sqrt{3}} \frac{e^6}{C^3(2\pi M)^{3/2}} \frac{N_e^2}{(kT)^{1/2}} e^{-h\nu/kT} \times \left[g_{ff} \exp\left(\frac{X_i/l^* - \Delta X_i}{kT} \right) + \frac{2X_i}{kT} \sum_{n=n^*}^{n=l^*-1} \frac{g_{fb}}{h^3} \exp\left(\frac{X_i/n^2 - \Delta X_i}{kT} \right) \right] + \frac{2h\nu^3}{C^2} e^{-h\nu/kT} N_H \sigma_{H^-}, \quad (2)$$

where g_{ff}, g_{fb} are the Gaunt factors for free-free and free-bound transitions, X_i is ionization energy, ΔX_i is lowering of the ionization potential, and σ_{H^-} is the absorption cross section for absorption by H^-. The other symbols have their usual meaning. Given the species, wavelength, and electron temperature, plus the measured continuum intensity, one can invert Eq. (2) to determine the electron density. Absolute-intensity calibration was performed using a tungsten ribbon lamp.[12] Comparison (see Fig. 4) of the electron density decay as measured by the two techniques shows agreement to within 10% at all times. The slightly different decay rate using the two methods is well within combined experimental uncertainties.

In the profile analysis, the electron density as measured by the interferometer was used owing to its freedom from any thermodynamic assumptions. Estimated average accuracy for the interferometric density is ±7%.

C. Profile measurement

Stark profiles were measured using a 0.5-m Ebert scanning spectrometer. Each profile was scanned on a shot-to-shot basis, beginning on the red wing and moving in variable steps across the profile. Four shots were taken at each step to provide a meaningful average and standard deviation. The steps range from 10 Å on the far wing to 0.25 Å in the center. Estimated wavelength error did not exceed 1 Å over an entire profile and 0.05 Å per step.

The instrumental profile was measured using the 6328-Å line of a low-power He-Ne laser. The high intensity of the laser line allowed us to accurately measure the far-line wings. Figure 5 shows the instrumental profile used in the reduction of all data. As a precaution against any wavelength dependence of this profile, several lines from a low-density discharge tube at lower wavelengths were measured, revealing no significant wavelength dependence.

An RCA 7265 photomultiplier with a cathode to anode potential of 2500 V was used as the detector. The output signal was terminated in a high-gain oscilloscope with high-frequency filters. Frequent checks of the oscilloscope calibration showed no significant variation during the data-collection

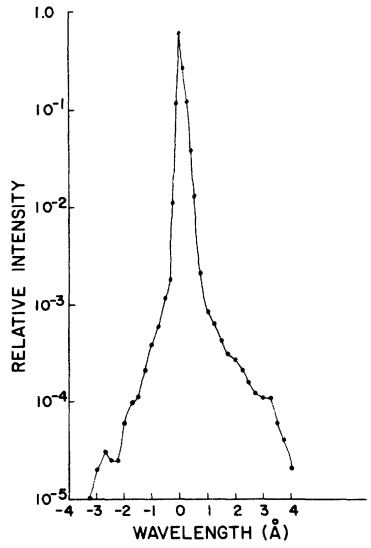

FIG. 5. Instrumental function used in the convolution of theoretical profiles.

period. The photomultiplier gain was assumed to be linear; a check with optical filters indicated less than a few percent variation in gain.

The optical system was absolutely calibrated for three different wavelengths spanning each profile using a tungsten ribbon lamp operated at conditions specified by Stair *et al.*[12] A second-order polynomial in wavelength was defined by these three points so that the calibration at any wavelength could be defined. Variation in the calibration factor was no more than a few percent for the various points across any one profile.

A measurement[8] of the optical depth of the plasma was made by placing a plane front surface mirror behind the plasma along the line of sight of the monochrometer, as described by Cooper.[13] Only H_α and H_β were found to be significantly absorbed.

III. RESULTS AND DISCUSSION

The presence of strong magnetic fields can significantly perturb and distort line profiles because of the quasistatic Zeeman effect superimposed on the Stark-effect profiles.[14] The 500-G field used in this experiment should not cause any distortion in the observed profile. Wavelength splitting due to the Zeeman effect is much less than the observed Doppler and Stark widths. The average Stark shift for an electric field strength $F_0 = (4\pi N/3)^{2/3} e/4\pi\epsilon_0$, is a factor of 10 larger than the Zeeman shift for our 500-G field. Electron gyrofrequency is well below the plasma frequency, so that the straight-line approximation for perturber paths used in the theories[6,7] may be assumed valid. Other effects on the line profiles such as electrodynamic line broadening[15] and polarization of the microfield should be much smaller than any observable phenomena.

Experimental and theoretical Stark profiles for the lines H_β to H_{10} were compared both graphically and numerically. Theoretical profiles were constructed by folding the theoretical Stark profiles with a Doppler and instrumental function, which accounted for the finite temperature of the radiators and distortions from the monochrometer. The profiles of Kepple and Griem[7] were extended to the far-wing points by assuming a $\frac{5}{2}$ slope from the last calculated point, rather than using the asymptotic wing formula. A temperature of 10 000 °K was used for the Doppler profiles. Other temperatures for the neutrals, such as 5000 and 20 000 °K, were tried, but there was no significant difference in the final profiles.

Both the experimental data and theoretical profiles were normalized to unity and displayed on log-log plots. Plots were normalized using a modified Simpson integration technique. In order to plot the experimental data in this manner, one must have a method for selecting the center of the experimental profiles. In this analysis, the centering procedure described by Wiese *et al.*[2] was used; namely, the center is defined as the best fit bisecting the $\frac{1}{2}$, $\frac{1}{4}$, and $\frac{1}{8}$ widths.

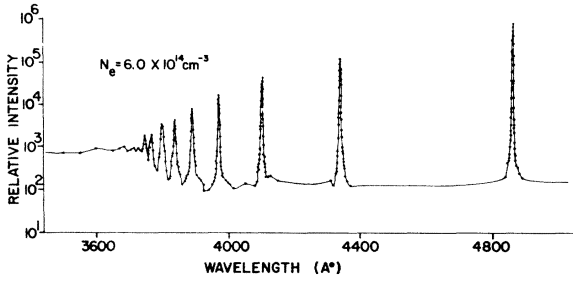

FIG. 6. Balmer spectrum at an electron density 6×10^{14} cm^{-3}.

Figure 6 shows, on a semilog plot, spectral intensity data for the Balmer spectrum at a single density. This spectra contains data taken over a period of several months put on single intensity scale using the daily intensity calibrations to normalize. Each point on the plot is an average of four shots. The data span an intensity range of a factor of 10^4. The scatter in the data does not become appreciably worse at the lower intensity levels. A simple Inglis-Teller estimate of the last observable line suggests we should see one more line than we can easily distinguish.

For the purpose of observing the scaling with principal quantum number, the average deviation between the experimental intensity at a given wavelength and the theoretical intensity at the same wavelength was computed and averaged for all densities of all lines. The deviation for each pro-

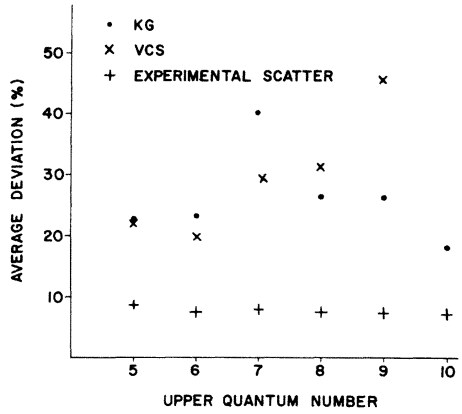

FIG. 7. Comparison of the average deviation of experimental and theoretical profiles, as calculated by Vidal, Cooper, and Smith, and Kepple and Griem. Standard deviation of the mean experimental scatter is also given.

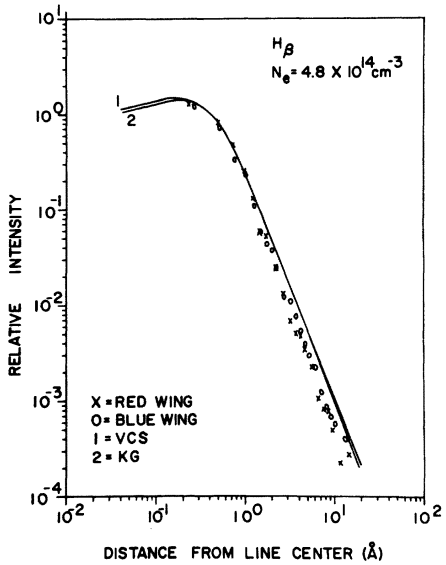

FIG. 8. Experimental profile of H_β.

file at each density was defined as

$$\delta = \sum_{i=1}^{N} \frac{1 - I_{av}(\lambda_i)/I_{th}(\lambda_i)}{N}, \tag{3}$$

where N is the number of points for a given profile, I_{av} is the average value of intensity from four shots, and $I_{th}(\lambda_i)$ is the intensity calculated by either KG or VCS theory at the wavelength λ_i. Theoretical and experimental profiles were always compared with equal areas. Results, along with the fractional standard deviation of the mean for the experimental data, are shown in Fig. 7. There was not a significant trend in the comparison between theory and experiment with respect to density. The best agreement between theory and experiment is 20%, which is somewhat larger than would be expected from shot-to-shot reproducibility in the experiment. For the lower quantum number ($n = 5, 6$) there is little difference between the results of Kepple and Griem[7] and Smith, Cooper, and Vidal,[6] while for the higher lines, the VCS calculations diverge. One possible cause for this discrepancy is that only the function $G_1(S,X,U)$ was included in these high-quantum-number calculations.[6,16] Other terms such as $G_2(S,X,U)$ may cause significant changes. The larger deviation for both theories for H_ϵ is probably due to experimental difficulties with H_ϵ data. The absolute intensity of H_ϵ also showed anomalous behavior.

In the following figures we present representative individually measured line profiles and compare them with the calculated profiles of Kepple and Griem[7] and Smith, Cooper, and Vidal.[6] Measured red and blue wings are indicated by the symbols × and ○, respectively.

A. H_β

A representative profile for H_β is displayed in Fig. 8. The basic features of the H_β profiles are (i) the measured profiles are always narrower in the wings than theoretical profiles and (ii) the wings appear to approach a $\frac{5}{2}$ slope in the wings faster than calculated. The discrepancies were slightly larger at the higher densities, probably because the core structure is more pronounced. Since the experimental and theoretical profiles are normalized to the same area, one can not separate the effects of a core disagreement and disagreement on the wings. Optical depth corrections at the center of H_β increased the peak intensity by as much as 50%. Because of the uncertainties connected with optical depth correction, we do not feel that these profiles provide an accurate comparison with theory, and include the H_β profiles only for their qualitative information.

In an experiment at 10^{15} cm^{-3}, Burgess and Mahon[17] found the experimental structure in the center of H_β to be much less pronounced than theory would predict. Our data are not sufficiently fine grained to verify their findings, but they do suggest similar results.

B. H_γ

Figures 9 and 10 show a sample of H_γ data displayed in a logarithmic format. Wing agreement on

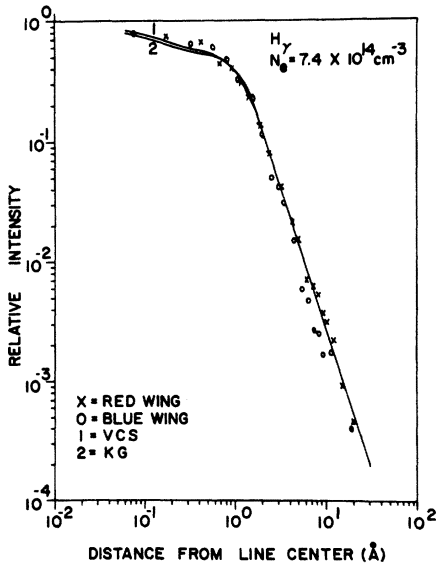

FIG. 9. Experimental profile of H_γ at an electron density 7.4×10^{14} cm^{-3} compared with theoretical profiles.

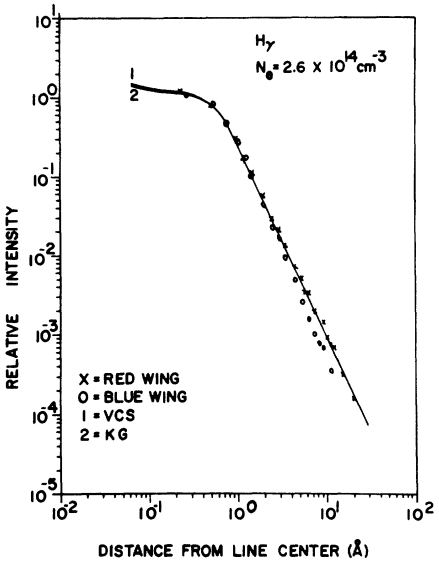

FIG. 10. Experimental profile of H_γ at an electron density 2.6×10^{14} cm^{-3} compared with theoretical profiles.

the average is excellent, and the blue wing is consistently lower than the red wing. The scatter of our data and estimates of possible systematic errors suggest that the difference between the red and blue wings is significant and can not be attributed solely to experimental errors. The central features of the line profile fit well with the theoretical calculations.

Another method of comparing line profiles is to compare the density measured interferometrically

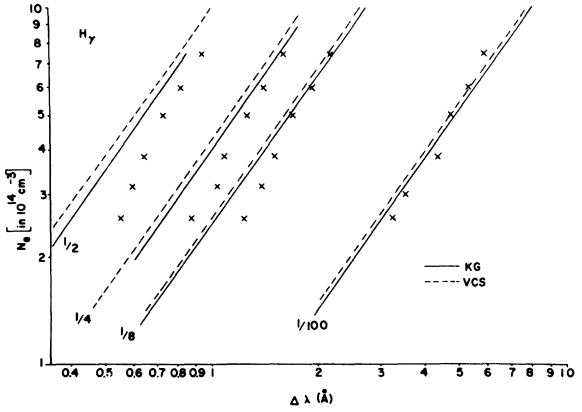

FIG. 12. Fractional widths of H_γ as a function of electron density. Uncertainty in experimental data is ±0.2 Å.

with that obtained from a best fit to the complete line profile. We defined the best fit to a line profile as the minimum value of the quantity δ as defined in Eq. (3). A comparison of the densities obtained from minimizing the deviation between theory and experiment, and from interferometric results, is shown in Fig. 11. Using the entire line profile for minimization tends to weight line wings preferentially, but minimizing only the experimental points with a factor of 100 of peak intensity gave essentially the same results. The maximum difference between the H_γ and interferometric density occurred at the highest densities and was 14% lower for KG theory and 9% low for VCS theory. This is the density region where the interferometer

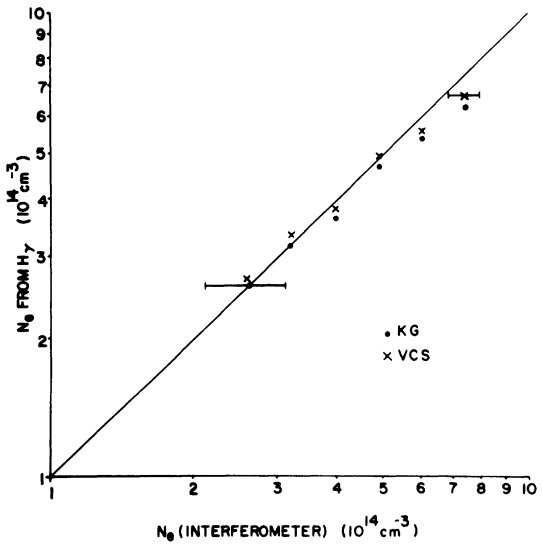

FIG. 11. Comparison of electron density obtained from interferometric measurements and from minimizing the deviation to H_γ profiles.

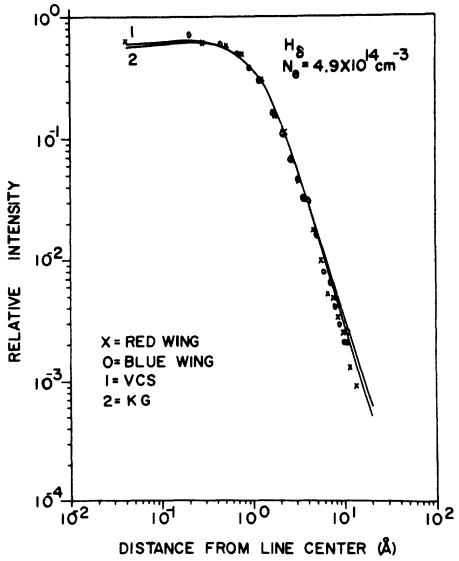

FIG. 13. Experimental profile of H_δ at an electron density 4.9×10^{14} cm^{-3} compared with theoretical profiles.

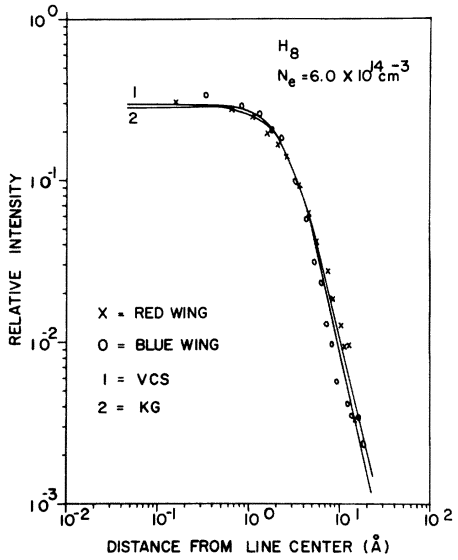

FIG. 14. Experimental profile of H_8 at an electron density 6.0×10^{14} cm^{-3} compared with theoretical profiles.

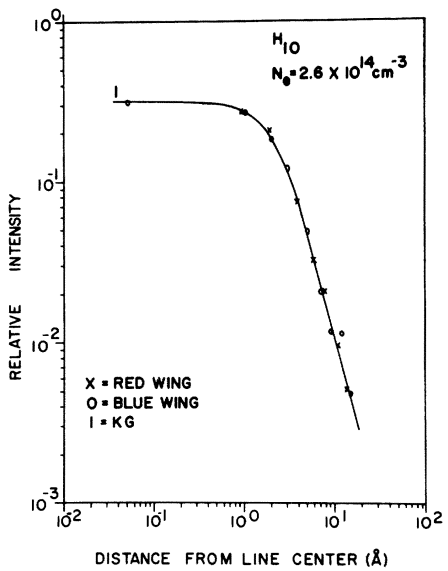

FIG. 16. Experimental profile of H_{10} at an electron density 2.6×10^{14} cm^{-3} compared with theoretical profile by Kepple and Griem.

data should be most accurate. The accuracy in defining a density from the minimization technique is better than 2%. The observation of lower electron densities from the minimization technique is qualitatively in agreement with the recent observations of Evans *et al.*[4] At densities below 5×10^{14} cm^{-3}, the two methods of measuring density agree to well within experimental errors.

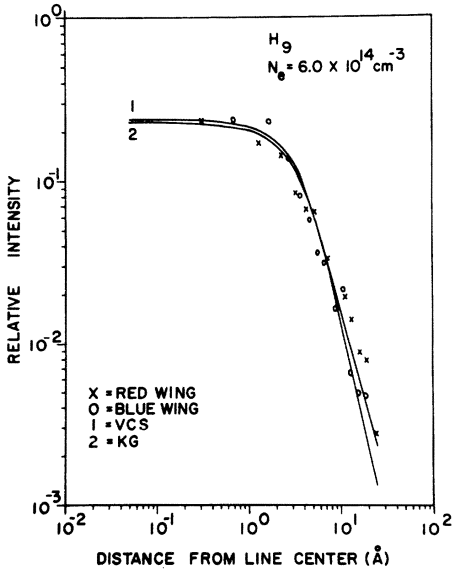

FIG. 15. Experimental profile of H_9 at an electron density 6.0×10^{14} cm^{-3} compared with theoretical profiles.

Traditionally, line widths have been used to compare profiles. In Fig. 12, we show fractional widths of H_γ as a function of interferometric electron density. Theoretical line widths were found from the final convoluted profiles, to prevent any influence of the Doppler or instrumental profiles. Experimental widths were found by a linear interpolation between the two points surrounding the fractional width. Error estimates for experimental widths range from 0.2 Å in the line center to 0.5 Å on the line wings. Theoretical and experimental widths are in agreement to within experimental error estimates although there is a suggestion of a trend for experimental line widths to be larger than theoretical widths, particularly at low densities. Widths at $\frac{1}{100}$ peak intensity agree well with that which would be predicted from the electron density features in Fig. 11.

C. H_δ

A sample of H_δ data is displayed in Fig. 13. Basic features of the profile are very similar H_β. Line centers always tended to be too high and wings too narrow. This feature was most noticeable at the higher densities. The experimental profiles seem to reach a $\frac{5}{2}$ slope on the wings sooner than predicted by theory. There is almost no indication of asymmetries in the line wings. No statement can be made for H_δ concerning the core structure since there are at most two or three points within the peaks of the structure.

D. Higher lines

Figures 14, 15, and 16 display samples of H_8, H_9, and H_{10} data. One interesting feature of the profiles is the fact that for all densities, the blue wing appears to be higher than the red in the core, but on the far line wings, the red wing becomes higher than the blue wing. The same phenomenon was observed by Wiese *et al.*[4] for H_β and H_γ in a high-density plasma. They traced the phenomenon to quadrapole interaction, as suggested by Sholin.[18]

For H_{10}, we determined the underlying continuum level by picking the continuum which would give a $\frac{5}{2}$ slope on the line wings. For all other lines we were able to measure the continuum level directly and substract it from the measured line intensities. The continuum estimated by the fit to a $\frac{5}{2}$ slope was in agreement with other continuum measurements.

IV. SUMMARY

Experimental profiles of the Balmer lines (H_β–H_{10}) have been measured over the density range $(2-8)\times10^{14}$ cm^{-3} and compared with theoretical profiles. Probe measurements showed that the plasma was homogeneous over 94% of its length. Electron densities as determined by minimizing the deviation between theoretical and experimental profiles were lower than the interferometric density at our upper density range and were in satisfactory agreement in the density range below 10^{14} cm^{-3}. Linewidths scaled with density as expected. Evidence for asymmetries in the far-line wings were noted.

ACKNOWLEDGMENTS

We would like to thank P. Neilsen and M. Machalek for use of equipment, and J. Burnside for aid in data reduction. We would also like to thank Earl Smith for calculating profiles of the higher Balmer lines. Stimulating conversations with J. Cooper and H. Griem are gratefully acknowledged.

---

*Research supported in part by the Welch Foundation, the National Science Foundation, and National Aeronautics and Space Administration.

† Present address: 1309 Windy Meadow, Plano, Tex. 75074.

[1] C. R. Vidal, Z. Naturforsch. A 19, 947 (1964); H. Schlüter and C. Avila, Astrophys. J. 144, 785 (1966); R. D. Bengtson, J. D. Tannich, and P. Kepple, Phys. Rev. A 1, 532 (1970).

[2] W. L. Wiese, D. E. Kelleher, and D. R. Paquette, Phys. Rev. A 6, 1132 (1972).

[3] R. A. Hill and J. B. Gerardo, Phys. Rev. 162, 45 (1967).

[4] D. L. Evans, D. P. Aeschliman, and R. A. Hill, Phys. Rev. A 10, 2450 (1974).

[5] A. E. Robson and J. Sheffield, in *Plasma Physics and Controlled Nuclear Fusion Research* (International Atomic Energy Agency, Vienna, Austria, 1969), Vol. 1, p. 119; P. E. Phillips and A. E. Robson, Phys. Rev. Lett. 29, 154 (1972).

[6] E. W. Smith, J. Cooper, and C. R. Vidal, Phys. Rev. 185, 140 (1969); J. Quant. Spectrosc. Radiat. Transfer 11, 263 (1971); Astrophys. J. Suppl. 25, 37 (1973).

[7] P. Kepple and H. R. Griem, Phys. Rev. 173, 317 (1968).

[8] G. R. Chester, Ph.D. thesis (The University of Texas, 1973) (unpublished).

[9] J. W. M. Paul, M. J. Parkinson, J. Sheffield, and L. S. Holmes, in *Proceedings of the Seventh International Conference on Phenomenon in Ionized Gases*, edited by B. Perovic and D. Tosic (Gradevinska Knjiga, Belgrade, 1966), Vol. II, p. 819.

[10] H. R. Griem, *Plasma Spectroscopy* (McGraw-Hill, New York, 1964).

[11] A. Eberhagen and W. Lünow, Institut für Plasmaphysik report No. IPP/6/20 (unpublished).

[12] R. Stair, R. G. Johnston, and E. W. Halbach, J. Res. Nat. Bur. Stand. (U.S.) A 64, 291 (1960).

[13] J. Cooper, Rept. Prog. Phys. 29, 35 (1966).

[14] H. W. Drawin, H. Henning, L. Herman, and Nguyen-Hoe, J. Quant. Spectrosc. Radiat. Transfer 9, 317 (1969).

[15] Ya. I. Galushkin, Astron. Zh. 47, 375 (1970) [Soviet Astron. 14, 301 (1971)].

[16] J. Cooper (private communication).

[17] D. D. Burgess and R. Mahon, J. Phys. B 5, 1756 (1972).

[18] G. V. Sholin, Opt. Spektrosk. 26, 489 (1969) [Opt. Spectrosc. 26, 275 (1969)].